# Droplet vorticity alignment in model polymer blends

K. B. Migler[a)]

*Polymers Division, National Institute of Standards and Technology, 100 Bureau Drive, Gaithersburg, Maryland 20899-8542*

(Received 21 June 1999; final revision received 29 November 1999)

**Synopsis**

We utilize stroboscopic optical microscopy to monitor the shear induced deformation of polymeric droplets in an immiscible polymeric matrix and find that under conditions of high droplet elasticity, the droplets can align in the vorticity direction. We consider the case where the viscosity ratio of the two phases is near unity but the elasticity ratio of the droplet to the matrix is greater than 100. This is achieved by using a matrix phase of polydimethylsiloxane and a droplet phase of a polyisobutylene based ''Boger'' fluid. In the limit of weak shear and small droplets, the droplet alignment is along the shear direction, whereas for strong shear and large droplets, the alignment is along the vorticity direction. There is a range of conditions for which alignment can be along either axis. For droplets aligned along the vorticity axis, the distribution of aspect ratios is broad. The kinetic transformation from droplet flow alignment to vorticity alignment upon increase of shear flow has been observed, as well as the relaxation back to a spherical shape upon cessation of shear. We deduce from the kinetic experiments that the thickness in the gradient direction is less than that in the flow and vorticity directions. © *2000 The Society of Rheology.* [S0148-6055(00)00202-9]

## INTRODUCTION

The success of the polymer blends industry is based on the synergistic enhancements in physical properties that can be achieved by blending immiscible materials. The blending typically occurs during extrusion under conditions of high stress, where the minor component is broken up into micron-sized droplets or sheets [Manas-Zloczower and Tadmor (1994)]. The morphology and size of the dispersed phase are critical to the ultimate mechanical properties [Meijer *et al.* (1988)].

The fundamental understanding of droplet shape and breakup is based on the work of Taylor (1932) and (1934) and Tomatika (1935), who found the two dimensionless parameters that control the behavior. The first parameter is the viscosity ratio between the two phases;

$$\lambda = \eta_d/\eta_c, \tag{1}$$

where $\eta_d$ and $\eta_c$ are the viscosities of the droplet and continuous phases, respectively. The second dimensionless parameter is the capillary number

$$\mathrm{Ca} = \frac{\eta_c \dot{\gamma} R_0}{\kappa}, \tag{2}$$

a)Electronic mail: kalman.migler@nist.gov

where $\dot{\gamma}$ is the shear rate of the matrix, $R_0$ is the radius of the unperturbed droplet, and $\kappa$ is the interfacial tension. The capillary number is a measure of the ratio of the viscous to interfacial stresses. There exists a critical capillary number $Ca_c$, which determines the stability of a droplet in a flow field; it is a function of both $\lambda$ and the type of flow. For pure shear flow, the shape of the curve $Ca_c$ vs $\lambda$ is well known; for $\lambda \approx 1$ it has a minimum at $Ca_c \cong 0.5$, for $\lambda > 4$ it becomes infinite so that droplets are stable at all capillary numbers, and for $\lambda < 0.1$ it increases in a power law fashion [Bentley and Leal (1986a); Bentley and Leal (1986b); Cox (1969); Grace (1982); Stone (1994)].

However, it is well known that polymeric blends do not follow the simple behaviors predicted by the Taylor theory [Cigana *et al.* (1997); Elmendorp and Vandervegt (1986); Favis (1994); Favis and Chalifoux (1987); Ghodgaonkar and Sundararaj (1996); Gonzalez Nunez *et al.* (1993); Gonzalez-Nunez *et al.* (1996); Mekhilef *et al.* (1997); Scott and Macosko (1995); Sundararaj *et al.* (1992); Sundararaj *et al.* (1996); Vanoene (1972)]. An important component in this discrepancy is the elasticity of the polymeric materials (other components are coalescence and complex flow fields). Vanoene (1972) first considered the effects of viscoelasticity and proposed that an additive term proportional to the normal stress differences between the droplet and matrix phases be added to the interfacial term of Eq. (2). To understand elasticity, experiments have focused on direct visualization of droplets under shear flow. Elmendorp and Maalcke (1985) found that as the elasticity of the droplet phase is increased, the shear induced deformation and breakup of the droplets is reduced. Conversely, they found that as the matrix elasticity is increased, droplet deformation is enhanced and breakup more readily occurs. Flumerfelt (1972) studied the breakup of Newtonian drops in a viscoelastic matrix and found that increasing elasticity of the continuous phase tends to increase the critical shear rate required for breakup. Gauthier *et al.* (1971), studied the effects of viscosity ratio and viscoelasticity and found that at low viscosity ratio, viscoelastic droplets behave in a manner similar to Newtonian ones. However, at higher viscosity ratio, the droplets are pulled into threads as they breakup, and the resulting $Ca_c$ is much greater. Varanasi *et al.* (1994) utilized a Boger fluid for the droplet so that the effects of viscosity ratio and elasticity could be separated. They found that $Ca_c$ is linear with the calculated primary normal stress difference of the droplet, and also found interesting shear and viscosity ratio effects.

Most processing work involves viscoelastic drops in a viscoelastic matrix. Mighri *et al.* (1998) extended the above works by studying the effects of model viscoelastic drop in a viscoelastic matrix. Migler *et al.* (1999) studied the deformation of polystyrene drops in a polyethylene matrix as they were extruded through an optical slit die located at the end of a twin screw extruder. They found a transition from ellipsoidal droplets at low capillary number to strings at modest capillary number and back again to spheres (of the same size as found under low capillary number conditions). Droplet viscoelasticity was believed to play a role in this transition.

In some cases, remarkable effects have been observed along the vorticity axis. Levitt *et al.* (1996) studied the kinetics of droplet breakup and deformation; in the initial stage of the process, it can become wider in the vorticity direction than the original droplet. Eventually, the elongation in the flow direction forces the diameter to decrease. This transient vorticity widening was attributed to second normal forces in the matrix.

In the case of fibers in a viscoelastic flow field, it was observed by Gauthier *et al.* (1971) that fibers orient along the vorticity axis when placed in either viscoelastic or pseudoplastic fluids. Leal (1975) presented a theoretical analysis of rod-like particles in a second order fluid and found that normal stress differences can sometimes produce this orientation.

Recently, Hobbie and Migler (1999) found that the deformation of polystyrene droplets in a polyethylene matrix in the plane containing the flow and flow gradient directions had a peak as a function of shear. In two of the three blends, the droplets transformed from alignment along the flow axis at low shear to alignment along the *vorticity axis* at the highest shear stresses near the wall. Rheological data showed that the normal forces in the droplet were less than that of the matrix at low shear, but extrapolation of the data to high shear (the region in which vorticity alignment was observed) indicated a crossover in which the droplet normal forces exceed that of the matrix.

Searching the literature, we find one other example of droplet vorticity alignment. Bartram *et al.* (1975) studied a ''blend'' of a 5% aqueous solution of polyacrylamide in a 3% aqueous solution of polyacrylamide. Before the droplets dissolved, they were sheared and were observed to elongate and breakup along the vorticity axis. In their second example a Guar gum solution in a PAA solution was studied and a somewhat similar finding was reached. Due to osmotic pressure difference between the two materials, the composition of these phases may also vary with time. Comparison to the results of Hobbie and Migler is difficult because Bartram's textual description does not contain data or photographs and reports minimal rheology.

In this work, we seek to reproduce, under carefully controlled laboratory conditions, the vorticity alignment phenomena that were observed previously. Hence, we work with a transparent rotating plate–plate device to generate simple shear flow. Based on the results of Hobbie and Migler (1999) in which the droplet normal force was believed to play a key role, we choose a blend in which the droplet normal force greatly exceeds that of the matrix. For the droplet phase, we use a non-shear thinning highly elastic fluid; a polyisobutylene (PIB) based Boger fluid. The matrix is polydimethylsiloxane (PDMS) which is also non-shear thinning and has much weaker normal forces at comparable shear rates. An additional advantage of these materials is that the elasticity of the Boger fluid, as well as the viscosities of both materials, is easily varied over a wide range.

## EXPERIMENT

The quartz shearing apparatus has been described in detail by Kim *et al.* (1996). It consists of a rotating upper plate of 8 cm diameter and a fixed bottom plate of larger diameter. The optics is configured for nearly simultaneous optical microscopy and optical light scattering, although in this experiment we utilize only the microscopy in bright field mode. Depending on the microscope objective, the field of view ranges from 200 $\mu$m to 1.5 mm. The observation point is located at a radial distance of 25 mm from the axis of rotation, so the shear rate gradient within a given field of view is small. The gap width used here is 0.47 mm. Stroboscopic illumination is synchronized to a video camera to allow visualization of fast moving objects. Video is recorded onto S-VHS tape for subsequent analysis. A sketch of the instrument and the geometry of the experiment instrument is shown in Fig. 1.

The PDMS was purchased from Gelest (DMS-T43, 30000 cSt) and was used as received. (Certain commercial equipment, instruments, or materials are identified in this paper in order to adequately specify the experimental conditions. Such identification does not imply recommendation by the National Institute of Standards and Technology, nor does it imply that the materials are necessarily the best available for the purpose.) A Boger fluid of $1\times10^{-3}$ mass ratio of high molecular weight PIB in a low molecular weight PIB was prepared as follows. High molecular weight PIB from Aldrich (average $\mathrm{Mw} = 4.6\times10^{6}$), was placed in hexane at a mass ratio of $1.0\times10^{-3}$. The solution was slowly stirred with a magnetic stir bar at room temperature for 2 d, well beyond the point

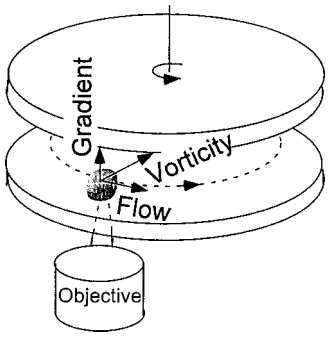


**FIG. 1.** Schematic of the transparent plate-plate shearing apparatus showing a typical droplet. Drawing not to scale.

at which the PIB was visible. The high molecular weight PIB solution was then mixed with 800 Mw PIB (Aldrich) to achieve the desired mass ratio. The sample was poured into a shallow Petri dish and the hexane was allowed to evaporate at room temperature for 4 d. The sample was then placed in a vacuum oven overnight to remove residual hexane. The final mass fraction of hexane was 0.025. Optically, the sample appears clear, indicating that the sample is homogenous at the micron length scale.

Dilute emulsions of the Boger fluids in the PDMS matrix are prepared by weighing out the components into a glass vial and then gently mixing with a spatula by hand. The emulsion is prepared with a mass fraction of Boger fluid of 1% so that the interaction between droplets is minimized and to allow for easy visual identification of the droplets. The emulsion is allowed to sit overnight so that long filaments formed during the mixing process have time to relax into spherical droplets by either breakup or retraction. Air bubbles created during the mixing are removed by placing the sample in a vacuum for several hours. This mixing procedure produces droplets over a broad range of sizes from $1\mu$m to 0.5 mm.

## RHEOLOGY

Boger fluids were developed in 1977 and are composed of a small weight fraction of a very high molecular weight polymer dissolved in a viscous Newtonian solvent [Boger (1977)]. The viscosity of the mixture is controlled to a large extent by the solvent; thus the fluid is nonshear thinning. Although the weight fraction of the high molecular weight component is small, it causes substantial normal forces to be generated in the fluid. These fluids have been widely used as models for the Oldroyd-B constitutive equation [Boger and Mackay (1991)], in situations where one needs to separate shear thinning from elasticity [Larson (1988); Mighri *et al.* (1997)], and as model fluids in which to study flow instabilities [Shaqfeh (1996)].

The rheological data were taken on an ARES rheometer from Rheometric Scientific, using a 50 mm diam cone and plate setup, at room temperature, the cone angle was 0.02 rad. The steady state rheological data are shown in Fig. 2. The PDMS zero shear viscosity is $29.7\pm0.2$ Pa s and is fairly Newtonian for shear rates less than 40 $s^{-1}$. It exhibits measurable normal force at shear rates above 10 $s^{-1}$. For the PIB Boger fluid, the viscosity is nearly constant over the range shown changing from 19 Pa s at 0.1 $s^{-1}$ to 17.8 Pa s at 5 $s^{-1}$. Thus the viscosity ratio is $\lambda = 0.64$. This low shear value is 1.7 times that of the bare 800 Mw PIB of 11.3 Pa s. The PIB normal force is fit to $N_1 \approx \Psi_1 \dot{\gamma}^2$ for $\dot{\gamma} < 10\ s^{-1}$, where $\Psi_1$ is the first normal stress coefficient ($\Psi_1 = 48\pm1.5$ Pa $s^2$). At the

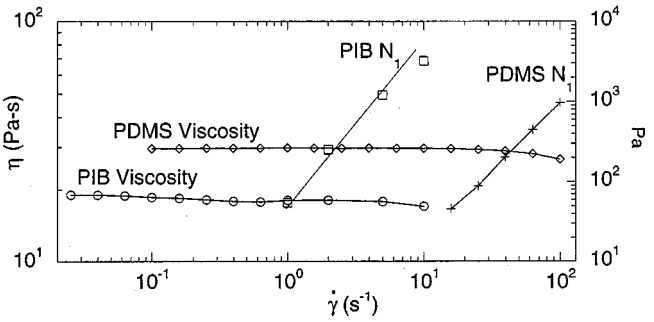


**FIG. 2.** Steady state rheology of PIB and PDMS at room temperature.

highest reported shear rate ($\dot{\gamma} = 10\ s^{-1}$), a rheological instability was found at long times; a sudden increase in the viscosity and normal force in a fashion similar to that observed by Magda and Larson (1988) and predicted by Phan-Thien (1983), (1985); its onset is geometry dependent. (The datum shown for PIB at $\dot{\gamma} = 10\ s^{-1}$ was the value of a local minimum before the sudden increase.) We can see that for comparable shear rates, for example $\dot{\gamma} = 1\ s^{-1}$, the PIB normal force is approximately 150 times greater than that of the PDMS. For each material, we can examine the characteristic shear rate $\dot{\gamma}^*$ at which the normal stress exceeds the viscous stress via $\eta\dot{\gamma}^*/N_1 = 1$. We find that $\dot{\gamma}^* = 0.42\ s^{-1}$ for the PIB and $\dot{\gamma}^* = 420\ s^{-1}$ for the PDMS, indicating the shear rate at which the normal stress becomes significant.

Based on the Oldroyd-B constitutive equation [Larson (1988)], we can associate $\Psi_1$ with a relaxation time constant $\lambda$, via $\Psi_1 = 2\lambda\eta_p$, where $\eta_p$ is the polymeric contribution to the viscosity, taken as the difference between the Boger fluid viscosity with that of the solvent. Using the measured value of $\Psi_1 = 48 \pm 1.5\ Pa\,s^2$ and $\eta_p = 8.6 \pm 0.2$ Pa s, we obtain $\lambda = 3.1$ s. Alternatively, we can measure the decay of the first normal force upon cessation of shear to obtain a relaxation time [Magda and Larson (1988)]; [Baumert and Muller (1995)]. In Fig. 3(A), we fit the data to a two exponential fit with time scales of $t_1 = 3.9$ s and $t_2 = 28$ s. The amplitude of $t_2$ is slightly greater than that of $t_1$. Thus the shorter time scale correlates with that deduced by the equation $\Psi_1 = 2\lambda\eta_p$, but the longer one clearly indicates that more than one time scale is present. Long time scales on the order of 30 s were also observed upon start up of shear in the PIB [Fig. 3(B)]. At $\dot{\gamma} = 5\ s^{-1}$ we see an overshoot in the first normal stress. The time scales for the PDMS are significantly faster than those of the PIB. The steady state stresses for the PDMS are reached much more rapidly for the PDMS; the viscous stress is reached in 0.05 s and the normal force is reached in 1 s.

Shear heating effects are not expected to play a significant role. The maximum temperature variation within the sample scales as $\eta\dot{\gamma}^2/k$ which is less than 0.1 °C for most conditions reported here. The heating of the entire sample plus quartz plates structure is also not significant as reported by a thermocouple in contact with the bottom quartz plate.

## MORPHOLOGY

In this following experiment encompassing Figs. 3–6 we shear from $\dot{\gamma} = 0.5\ s^{-1}$ to $\dot{\gamma} = 80\ s^{-1}$ in seven steps; $0.5\ s^{-1}$, $2\ s^{-1}$, $5\ s^{-1}$, $10\ s^{-1}$, $20\ s^{-1}$, $40\ s^{-1}$, and $80\ s^{-1}$. At $\dot{\gamma} = 80\ s^{-1}$, we observe an instability by eye at the outer edge of the top plate. While this instability did not propagate into the sample, we did not obtain data above this shear

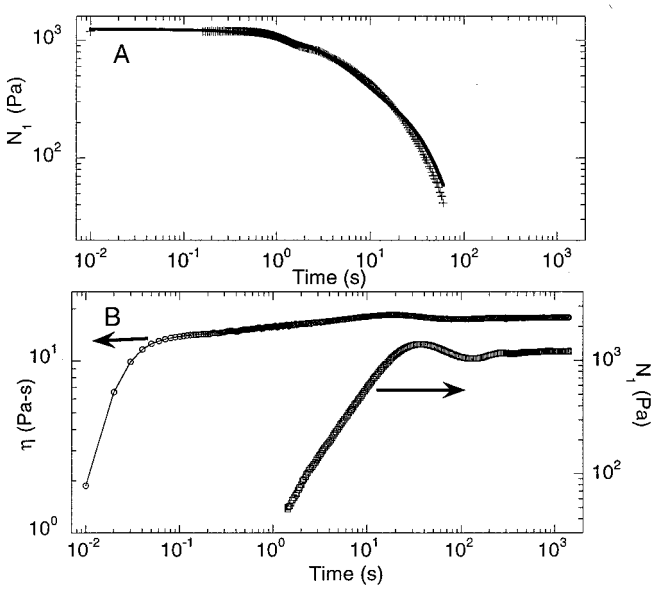


**FIG. 3.** Time dependent viscosity and normal force of the PIB Boger fluid upon (A) cessation of shear from $\dot{\gamma} = 5\ s^{-1}$, (B) commencement of shear at $\dot{\gamma} = 5\ s^{-1}$.

rate. The sample is maintained at each shear rate for 25 min before recording video data. At each shear rate, data are then taken at four magnifications in order to observe the morphology over the broad range of droplet sizes. The minimum droplet radius from which we can extract accurate aspect ratio data is approximately 5 $\mu$m. From one shear rate to the next, the shear is increased slowly over a period of approximately 1 min. In the data presented here, the objective lens is focused in the midplane of the sample. Droplets not in the midplane appear out-of-focus and move at a different velocity than those in-focus. In the aspect ratio measurements, only midplane droplets were used.

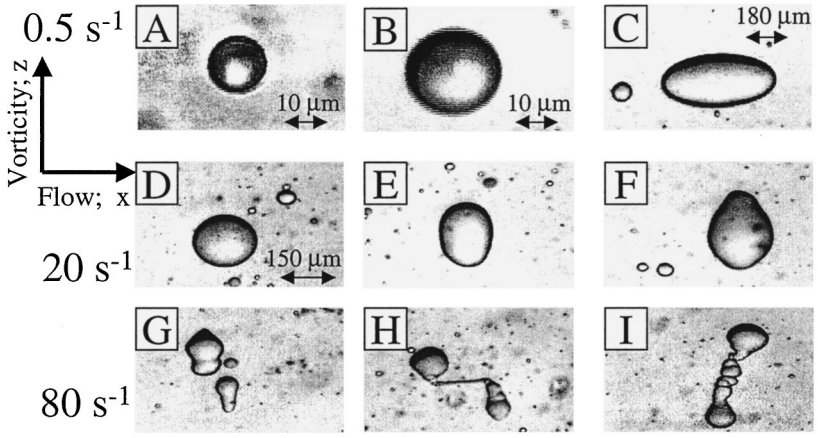


**FIG. 4.** Video micrographs of a PIB based Boger fluid in a PDMS matrix at a mass concentration of 1%. (A)–(C) $\dot{\gamma} = 0.5\ s^{-1}$, (D)–(F) $\dot{\gamma} = 20\ s^{-1}$, (G)–(I) $\dot{\gamma} = 80\ s^{-1}$. The flow direction is along the *x* axis and the vorticity direction is along the *y* axis. At a given shear rate, each picture corresponds to a different droplet. The field of view in (D)–(I) is the same.

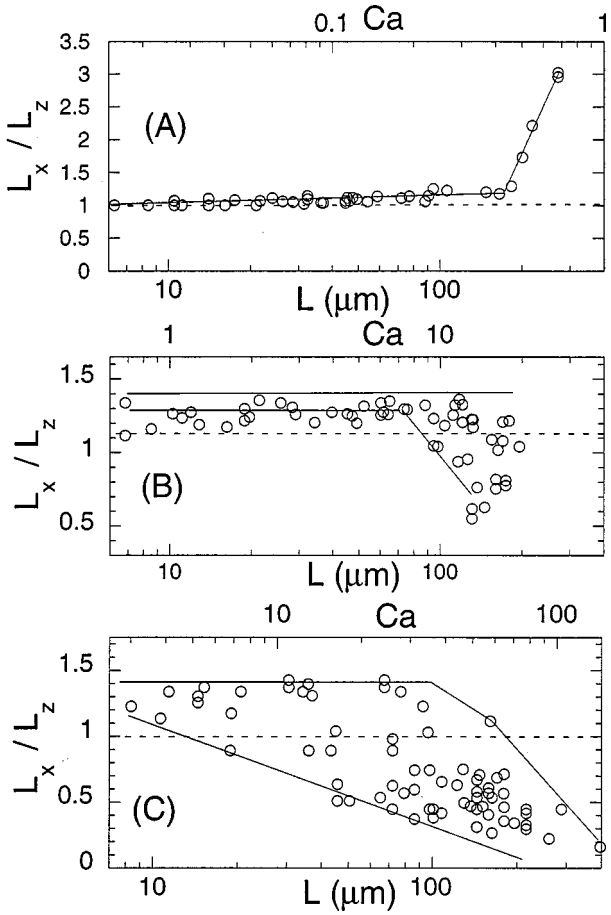


**FIG. 5.** Aspect ratio of the droplets as a function of capillary number for a fixed shear rate. (A) $\dot{\gamma} = 0.5\ s^{-1}$, (B) $\dot{\gamma} = 20\ s^{-1}$, (C) $\dot{\gamma} = 80\ s^{-1}$. $L_x$ ($L_z$) is the length of the droplet in the flow (vorticity) direction. The wide distribution of droplet sizes allows for the range of capillary numbers at fixed shear.

The morphology of the droplets at low shear rates is shown in Figs. 4(A)–4(C). Here we see weak elongation for the droplets whose width is 100 $\mu$m [Figs. 4(A) and 4(B)] and stronger elongation in Fig. 4(C), where the droplet size is much larger (note change in scale). We have measured the aspect ratio of a large number of droplets at each shear

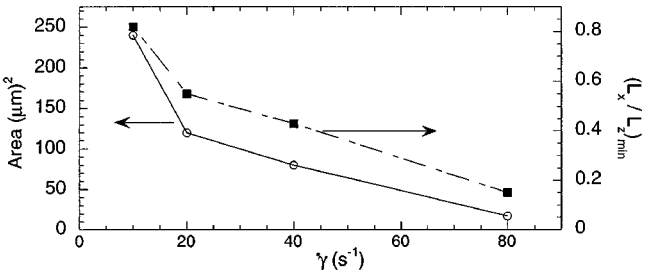


**FIG. 6.** At each shear rate, we plot the minimum droplet size that exhibits vorticity alignment and the droplet with the minimum $L_x / L_z$.

rate, and analyze the results in Fig. 5 as a function of capillary number and size. This method of varying capillary number contrasts with many other studies in which capillary number is varied by changing the shear rate for an individual droplet. Each point on a graph in Fig. 5 represents a measurement from a different droplet; the capillary number of that droplet is computed from Eq. (2) where the radius of the droplet is taken as that of the minor axis (in the flow–flow gradient plane). The interfacial tension is $\kappa = 3$ mN/M [Sigillo *et al.* (1997)]. The results for $\dot{\gamma} = 0.5\ s^{-1}$ are shown in Fig. 5(A). We plot the $x$ axis in terms of both the capillary number (top plot axis) and the diameter of the minor axis (bottom plot axis). We find weak elongation for $Ca < 0.4$ with a sharp upturn at higher capillary number. This upturn occurs at diameter in the vorticity axis of $L \approx 200\ \mu$m and we interpret it as a finite size effect. Large droplets will necessarily be squeezed by the plates into a disk-like shape. These droplets then show large extension along the flow axis. These large droplets breakup at larger shear rates as deduced by the absence of large droplets as shear is increased. At $\dot{\gamma} = 10\ s^{-1}$ (not shown), the aspect ratio as a function of capillary number is a constant value of 1.25 for droplets small enough that finite size is not an issue. There does exist a single large droplet that is aligned in the vorticity axis.

For the largest three shear rates used in this study, $\dot{\gamma} = 20\ s^{-1}$, $\dot{\gamma} = 40\ s^{-1}$, and $\dot{\gamma} = 80\ s^{-1}$, we find an increasing tendency for the droplets to align along the vorticity axis. Figures 4(D)–4(F) show micrographs for $\dot{\gamma} = 20\ s^{-1}$. Remarkably, we see three different droplets with similar cross sectional areas, but with very different shapes. These three shapes are typical of what we observe at this shear rate. Thus after 25 min of shearing, or a shear strain of $\gamma = 6 \times 10^4$, an equilibrium steady state morphology has not emerged, but rather we see a distribution of shapes. Figure 4(D) shows a droplet oriented along the flow axis with aspect ratio 1.24, Fig. 4(E) shows an ellipsoidal droplet oriented along the vorticity axis with aspect ratio 0.85, and Fig. 4(F) is an irregularly shaped droplet oriented along the vorticity axis.

Upon increasing the shear rate to $80\ s^{-1}$, we see an enhancement in vorticity alignment, as well as instabilities in the droplets. Figure 4(G) shows droplets oriented along the vorticity axis, in a fashion similar to that found in Figs. 4(D) and 4(E). However, Fig. 4(H) shows an apparent breakup of one droplet into two. The daughter droplets are aligned along the vorticity axis and are still connected by a thin string of Boger fluid. Presumably, these droplets will eventually separate further and the string will become thinner until it breaks up; this process has not been studied in detail. Figure 4(I) shows a droplet oriented along the vorticity axis, but its shape is highly irregular. The droplet has become twisted along its major axis. We note that at this shear rate, a flow instability at the outer edge of the plate-plate device can be observed by eye. However, this instability did not propagate inwards into the sample—in fact we can state that at the point of observation, the flow is laminar. As the droplets have rather distinctive, shapes, we can often identify the same droplet each time it reenters the field of view of the microscope. Thus while the particle travels 157 mm in the flow direction each time it makes a revolution and is seen in the microscope, it has moved less than 20 $\mu$m in the other two directions. At the larger shear rates, we occasionally observe chaining of two to four droplets along the vorticity axis, a phenomenon that we have not studied in detail.

The plot of the aspect ratio as a function of capillary number is revealing. We see in Fig. 5 the increasing tendency for vorticity alignment with increasing shear rate. The first feature to note in these three plots is that at low capillary number, the droplets are mildly elongated with an aspect ratio slightly larger than one. This is a manifestation of the droplet elasticity; in the absence of the high molecular weight component, the slope of

the curves would be far greater [Mighri *et al.* (1998)]. The droplets would be highly elongated and break up at capillary numbers on the order of one. The uniformity of the response of the droplets to the shear field at low capillary number indicates that the high molecular weight component polymer in Boger fluid is distributed uniformly. The most striking feature of the aspect ratio plots of Fig. 5 is the wide range of aspect ratios found for a given capillary number, as was seen visually in the video micrographs [Figs. 4(D)–4(F)]. For example, at a Ca = 13 in Fig. 5(B), aspect ratios from 1.4 to 0.4 have been observed. The solid lines simply encompass the range of aspect ratios that have been observed. For the highest shear rate, $\dot{\gamma} = 80\ s^{-1}$, the upper solid line has been drawn with a downward kink at the end indicating the observation that in the limit of high shear rate and droplet size, the particles do not align along the flow axis, but are oriented in the vorticity direction.

We know that finite size plays a role in the elongation of larger droplets at $\dot{\gamma} = 0.5\ s^{-1}$ [Fig. 5(A)]. Examination of Fig. 5(B) indicates that the finite size may be playing a role for the larger droplets that exhibit vorticity alignment. However, Figs. 5(B) and 5(C) do show many droplets that exhibit vorticity alignment that are small enough so that finite size is not significant.

In order to simplify the data shown in the aspect ratio plots, we extract two essential parameters. First, for a given shear rate, we find the smallest droplet (in terms of cross sectional area) that exhibits vorticity alignment and we also find the droplet with the smallest $L_x/L_z$ (i.e., most strongly aligned along the vorticity axis.) The results are shown in Fig. 6. With the exception of $\dot{\gamma} = 10\ s^{-1}$, these are not the same particle. As the shear rate increases, there is a clear trend; the diameter of droplets that exhibit vorticity alignment decreases while the extent of alignment along the vorticity axis increases.

We have also conducted limited experiments in which we invert the two phases, i.e., a weakly elastic droplet (PDMS) in an elastic matrix (PIB based Boger fluid). We utilize the same PIB based Boger fluid and PDMS as described in the previous experiments. At $\dot{\gamma} = 5\ s^{-1}$, we observe that the initial slope of the curve of aspect ratio versus capillary number is approximately 3.5, in contrast to Figs. 5(A) and 5(B) where the initial slope is near zero. At this shear rate, droplets with radius greater than approximately 50 $\mu$m deform rapidly into threads which eventually break up into small droplets. Vorticity alignment is not observed over the accessible range of shear rates and droplet sizes. However, the maximum accessible Ca is smaller due to the breakup of the droplets.

In the case where both components are nonelastic (i.e., using the bare 800 Mw PIB as the matrix), we did not observe vorticity alignment. We did however observe chaining of the droplets along the vorticity axis, similar to the what was briefly mentioned in the case of elastic droplets.

## KINETICS OF VORTICITY ALIGNMENT

We can gain insights into the nature of the vorticity alignment by measuring the kinetics of a droplet as it transforms from flow alignment to vorticity alignment. In order to monitor the formation of vorticity alignment, we employed the following procedure. First the sample was sheared at $\dot{\gamma} = 40\ s^{-1}$ for 6 min to break up the largest droplets and then at $\dot{\gamma} = 2.4\ s^{-1}$ for 150 min. Next we suddenly increase the shear to $\dot{\gamma} = 40\ s^{-1}$. As mentioned earlier, through subsequent frame by frame analysis of the video one can identify individual droplets each time they flow into the field of view of the microscope. One can then monitor the kinetics if the morphological evolution is sufficiently slow. Often the droplets slowly drift out of view as time progresses or one cannot be certain

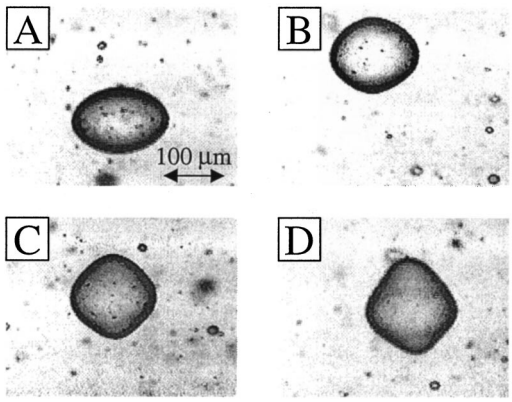


**FIG. 7.** Evolution of droplet morphology upon sudden increase of shear from $\dot{\gamma} = 2.4\ s^{-1}$ to $\dot{\gamma} = 40\ s^{-1}$. The droplet is imaged each time it comes into the microscope's field of view, which occurs in this case approximately every 17 s. The time is relative to the jump in shear rate. Width of each image is 383 $\mu$m. (A) $t = 13$ s; (B) $t = 159$ s; (C) $t = 259$ s; (D) $t = 330$ s. The axes are the same as in Fig. 4. The corresponding plot of aspect ratio vs time is shown in Fig. 8.

that one is following the same droplet; thus this technique is difficult. In Fig. 7 we show data from a case when we followed a droplet for 330 s that was observed to align along the vorticity axis following the shear jump from $\dot{\gamma} = 2.4\ s^{-1}$ to $\dot{\gamma} = 40\ s^{-1}$. For $t < 0$ s, we expect that the particle was weakly aligned along this axis due to the low shear rate. Figure 7(A) shows that at $t = 13$ s, it is still aligned along the flow axis. At $t = 159$ s, it is roughly circular in cross section. At $t = 259$ s we see that it is beginning to elongate along the vorticity axis, and at $t = 330$ s, it is elongated along the vorticity axis with $L_x/L_z = 0.90$. Figure 8 shows the evolution of morphology as a function of time. This plot indicates that the final aspect ratio has not been reached within this time frame.

We can determine that the thickness in the gradient direction is less than that in the other two directions. We infer information about the thickness in the gradient direction by measuring the cross sectional area as a function of time. From Figs. 7(A)–7(D), there is a relative increase in the cross sectional area of the droplet of 11%. At $t = 13$ s [Fig. 7(A)] we know that the thickness in the gradient direction is already less than that in either the flow or vorticity directions. Since the cross sectional area in the flow–vorticity

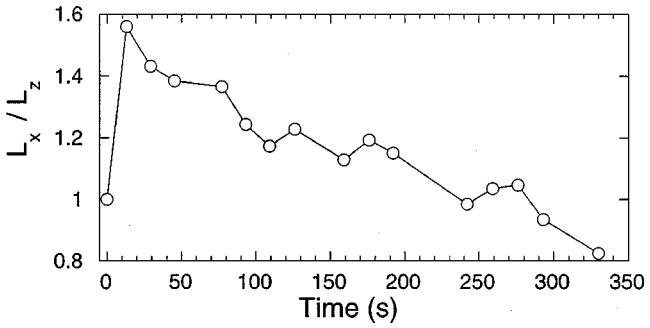


**FIG. 8.** Plot of the kinetics of vorticity alignment upon sudden increase of shear from $\dot{\gamma} = 2.4\ s^{-1}$ to $\dot{\gamma} = 40\ s^{-1}$. The corresponding video micrographs at four selected times is shown in Fig. 7.

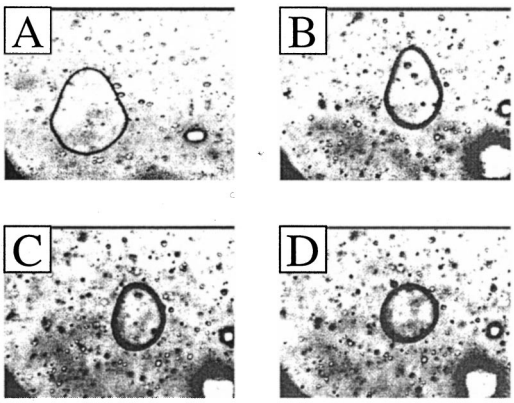


**FIG. 9.** Kinetics upon cessation of shear. In this case the viscosity of the matrix is 60 Pa s while we use the same PIB based Boger fluid. The axes are defined in Fig. 3. The following shear profile is used to obtain the sequence of micrographs; $\dot{\gamma}(t < 0) = 50\ s^{-1}$, next, $\dot{\gamma}(0s < t < 8s) \approx -2\ s^{-1}$, and finally $\dot{\gamma}(t > 8s) = 0\ s^{-1}$. (A) $t = -0.5$ s; (B) $t = 11$ s; (C) $t = 41$ s; (D) $t = 120$ s. Width of image is 600 $\mu$m.

plane increases upon vorticity alignment, from conservation of volume we conclude that the droplet becomes even thinner along the gradient axis during this process. Thus, assuming that the radius in the vorticity direction in Fig. 7(A) corresponds to that of the unperturbed droplet, we can say that the thickness in the gradient direction in Fig. 7 is roughly half that of the other two directions.

The relaxation of droplets upon cessation of shear can also be monitored. First, the sample is sheared at a high rate to induce vorticity alignment. Next the shear is turned off, and then the sample is sheared in the opposite direction (at a much lower absolute value than was used to induce the vorticity alignment) until one finds a droplet that is aligned along the vorticity axis. The relaxation from vorticity alignment to spherical is then monitored at $\dot{\gamma} = 0\ s^{-1}$. Figure 9 shows the case of the same PIB based Boger fluid as used previously but here we use a 60 Pa s PDMS matrix. Figure 9(A) shows the droplet during the initial high shear period ( $\dot{\gamma} = 50\ s^{-1}$ at a time 0.5 s before cessation of shear. Figure 9(B) shows the droplet immediately after it has been manually relocated. Figures 9(C) and 9(D) show the relaxation back to a spherical shape which occurs over a time frame of 60 s. Again, from conservation of volume constraints, we can conclude that the width of this droplet in the shear gradient direction is roughly half that in the vorticity direction. Although the cumbersome shear procedure employed here prevents a systematic study, we do find that the relaxation time is governed by the droplet size, indicating that surface tension plays a dominant role in this relaxation.

## DISCUSSION AND CONCLUSION

We have demonstrated that droplets can align along the vorticity axis under conditions where the viscosity ratio is near unity, but the elasticity ratio is of order 100. This phenomenon is observed for $Ca > 5$ in highly elastic droplets that are not broken up by the strong shear field. For $5 < Ca < 50$ we observe a bistability in the orientation, droplets can be aligned along either axis. For $Ca > 50$, we observe droplets aligned along the vorticity axis only. In a previous work in a polystyrene/polyethylene blend, we hypothesized that the normal forces in the droplets are responsible for the vorticity alignment. Intuitively, closed streamlines act as if they are under tension. In the rod climbing case, this tension causes the polymer to flow up the rod. In the case of droplets, closed

streamlines form in the flow/gradient plane and act to make the droplets expand in the vorticity direction. We recognize an alternative argument in which vorticity alignment is caused by the forces from the matrix, in the same way that fibers can align along the vorticity axis. One might argue that the long time scales of the droplet in regard to its normal forces would cause it to act particle-like under certain conditions and thus it would align along the vorticity axis. Clearly, the elasticity of the droplet causes the existence of droplets with large capillary numbers that otherwise would break up. However, we know that there is significant shear within the droplet because we have ascertained that it is thinner in this dimension than in the other two dimensions. Thus in order to maintain this shape, it must be under shear, hence a simple ''log rolling'' picture is incorrect. Although we do not know the shear rate in the droplet, the results from the Rheology section indicates that the normal forces from the droplet are expected to be substantial. A final argument for the importance of normal forces in the droplet is the time scale for the development of vorticity alignment after commencement of shear flow, which is of the same order of magnitude as the development of normal forces in the droplet.

While the droplet shown in Fig. 7 transforms its alignment from the flow to the vorticity axis, some others that are similarly sized do not. The reason for this lack of a steady state is unclear, but it does point to the possibility of an instability in which those which exhibit vorticity alignment are disturbed from their flow alignment shape, either by a breakup process or by collision with another droplet. In the case of droplet breakup, Fig. 4(H), we can see that the daughter droplets are aligned along the vorticity axis. After breakup, these droplets remain aligned along the vorticity axis. On the other hand, in the case of the droplet seen in Fig. 7, no disturbance is seen. We feel that the wealth of phenomena observed here coupled with the need for a quantitative understanding of the vorticity alignment mechanism leave room for much future work.

## ACKNOWLEDGMENT

The author gratefully acknowledges the assistance of C. C. Han, H. Jeon, C. Schultheisz, and J. F. Douglas.

## References

Bartram, E., H. L. Goldsmith, and S. G. Mason, ''Particle motions in non-Newtonian media III. Further observations in elasticoviscous fluids,'' Rheol. Acta **14**, 776–782 (1975).

Baumert, B. M. and S. J. Muller, ''Flow visualization of the elastic Taylor-Couette instability in Boger fluids,'' Rheol. Acta **34**, 147–159 (1995).

Bentley, B. J. and L. G. Leal, ''A computer-controlled 4-roll mill for investigations of particle and drop dynamics in two-dimensional linear shear flows,'' J. Fluid Mech. **167**, 219–240 (1986a).

Bentley, B. J. and L. G. Leal, ''An experimental investigation of drop deformation and breakup in steady, two-dimensional linear flows,'' J. Fluid Mech. **167**, 241–283 (1986b).

Boger, D. V., ''A highly elastic constant-viscosity fluid,'' J. Non-Newtonian Fluid Mech. **3**, 87–91 (1977).

Boger, D. V. and M. E. Mackay, ''Continuum and molecular interpretation of ideal elastic fluids,'' J. Non-Newtonian Fluid Mech. **41**, 133–150 (1991).

Cigana, P., B. D. Favis, C. Albert, and T. VuKhanh, ''Morphology-interface-property relationships in polystyrene/ethylene-propylene rubber blends. 1. Influence of triblock copolymer interfacial modifiers,'' Macromolecules **30**, 4163–4169 (1997).

Cox, R. G., ''The deformation of a drop in a general time-dependent fluid flow,'' J. Fluid Mech. **37**, 601–623 (1969).

Elmendorp, J. J. and R. J. Maalcke, ''A study on polymer blending microrheology. 1,'' Polym. Eng. Sci. **25**, 1041–1047 (1985).

Elmendorp, J. J. and A. K. Vandervegt, ''A study on polymer blending microrheology. 4. The influence of coalescence on blend morphology origination,'' Polym. Eng. Sci. **26**, 1332–1338 (1986).
Favis, B. D., ''Phase size interface relationships in polymer blends—The emulsification curve,'' Polymer **35**, 1552–1555 (1994).
Favis, B. D. and J. P. Chalifoux, ''The effect of viscosity ratio on the morphology of polypropylene polycarbonate blends during processing,'' Polym. Eng. Sci. **27**, 1591–1600 (1987).
Flumerfelt, R. W., ''Drop breakup in simple shear fields of viscoelastic fluids,'' Ind. Eng. Chem. Fundam. **11**, 312–318 (1972).
Gauthier, F., H. L. Goldsmith, and S. G. Mason, ''Particle motions in non-Newtonian media,'' Rheol. Acta **10**, 344–364 (1971).
Ghodgaonkar, P. G. and U. Sundararaj, ''Prediction of dispersed phase drop diameter in polymer blends: The effect of elasticity,'' Polym. Eng. Sci. **36**, 1656–1665 (1996).
Gonzalez-Nunez, R., B. D. Favis, and P. J. Carreau, ''Factors influencing the formation of elongated morphologies in immiscible polymer blends during melt processing,'' Polym. Eng. Sci. **33**, 851–859 (1993).
Gonzalez-Nunez, R., C. Fong, B. D. Favis, and D. DeKee, ''Deformation of drops in extensional viscoelastic flow,'' J. Appl. Polym. Sci. **62**, 1627–1634 (1996).
Grace, H. P., ''Dispersion of high viscosity immiscible fluid systems and the application of static mixers as dispersion devices in such systems,'' Chem. Eng. Commun. **14**, 225–277 (1982).
Hobbie, E. K. and K. B. Migler, ''Vorticity elongation in polymeric emulsions,'' Phys. Rev. Lett. **82**, 5393–5396 (1999).
Kim, S., J. W. Yu, and C. C. Han, ''Shear light scattering photometer with optical microscope for the study of polymer blends,'' Rev. Sci. Instrum. **67**, 3940–3947 (1996).
Larson, R. G., *Constitutive Equations for Polymer Melts and Solutions* (Butterworths, Boston, 1988).
Leal, L. G., ''The slow motion of slender rod-like particles in a second-order fluid,'' J. Fluid Mech. **69**, 305–337 (1975).
Levitt, L., C. W. Macosko, and S. D. Pearson, ''Influence of normal stress difference on polymer drop deformation,'' Polym. Eng. Sci. **36**, 1647–1655 (1996).
Magda, J. J. and R. G. Larson, ''A transition occurring in ideal elastic liquids during shear-flow,'' J. Non-Newtonian Fluid Mech. **30**, 1–19 (1988).
Manas-Zloczower, I. and Z. Tadmor, *Mixing and Compounding of Polymers: Theory and Practice* (Hanser, Munich, 1994).
Meijer, H. E. H., P. J. Lemstra, and P. H. M. Elemans, ''Structured polymer blends,'' Makromol. Chem., Macromol. Symp. **16**, 113–135 (1988).
Mekhilef, N., B. D. Favis, and P. J. Carreau, ''Morphological stability, interfacial tension, and dual-phase continuity in polystyrene-polyethylene blends,'' J. Polym. Sci., Part B: Polym. Phys. **35**, 293–308 (1997).
Mighri, F., A. Ajji, and P. J. Carreau, ''Influence of elastic properties on drop deformation in elongational flow,'' J. Rheol. **41**, 1183–1201 (1997).
Mighri, F., P. J. Carreau, and A. Ajji, ''Influence of elastic properties on drop deformation and breakup in shear flow,'' J. Rheol. **42**, 1477–1490 (1998).
Migler, K. B., E. K. Hobbie, and F. Qiao, ''In line study of droplet deformation in polymer blends in channel flow,'' Polym. Eng. Sci. **39**, 2282–2291 (1999).
Phan-Thien, N., ''Coaxial-disk flow of an Oldroyd-B fluid—exact solution and stability,'' J. Non-Newtonian Fluid Mech. **13**, 325–340 (1983).
Phan-Thien, N., ''Cone-and-plate flow of the Oldroyd-B fluid is unstable,'' J. Non-Newtonian Fluid Mech. **17**, 37–44 (1985).
Scott, C. E. and C. W. Macosko, ''Processing and morphology of polystyrene/ethylene-propylene rubber reactive and nonreactive blends,'' Polym. Eng. Sci. **35**, 1938–1948 (1995).
Shaqfeq, E. S. G., ''Purely elastic instabilities in viscometric flows,'' Annu. Rev. Fluid Mech. **28**, 129–185 (1996).
Sigillo, I., L. diSanto, S. Guido, and N. Grizzuti, ''Comparative measurements of interfacial tension in a model polymer blend,'' Polym. Eng. Sci. **37**, 1540–1549 (1997).
Stone, H. A., ''Dynamics of drop deformation and breakup in viscous fluids,'' Annu. Rev. Fluid Mech. **26**, 65–102 (1994).
Sundararaj, U., C. W. Macosko, R. J. Rolando, and H. T. Chan, ''Morphology development in polymer blends,'' Polym. Eng. Sci. **32**, 1814–1823 (1992).
Sundararaj, U., C. W. Macosko, and C. K. Shih, ''Evidence for inversion of phase continuity during morphology development in polymer blending,'' Polym. Eng. Sci. **36**, 1769–1781 (1996).
Taylor, G. I., ''The viscosity of a fluid containing small drops of another fluid,'' Proc. R. Soc. London, Ser. A **138**, 41–48 (1932).
Taylor, G. I., ''The formation of emulsions in definable fields of flow,'' Proc. R. Soc. London, Ser. A **146**, 501–523 (1934).

Tomotika, S., ''On the instability of a cylindrical thread of a viscous liquid surrounded by another viscous liquid,'' Proc. R. Soc. London, Ser. A, **150**, 322–337 (1935).

Vanoene, H., ''Modes of dispersion of viscoelastic fluids in flow,'' J. Colloid Interface Sci. **40**, 448–467 (1972).

Varanasi, P. P., M. E. Ryan, and P. Stroeve, ''Experimental-study on the breakup of model viscoelastic drops in uniform shear-flow,'' Ind. Eng. Chem. Res. **33**, 1858–1866 (1994).